TU Delft

Delft University of Technology

Effect of Activator and Mineral Admixtures on the Autogenous Shrinkage of Alkali-Activated Slag/Fly Ash

Ma, Yuwei; Gong, Jihao; Ye, Guang; Fu, Jiyang

DOI
10.3390/su152216101

Publication date
2023

Document Version
Final published version

Published in
Sustainability

Citation (APA)
Ma, Y., Gong, J., Ye, G., & Fu, J. (2023). Effect of Activator and Mineral Admixtures on the Autogenous Shrinkage of Alkali-Activated Slag/Fly Ash. *Sustainability*, *15*(22), Article 16101. https://doi.org/10.3390/su152216101

Important note
To cite this publication, please use the final published version (if applicable).
Please check the document version above.

Copyright
Other than for strictly personal use, it is not permitted to download, forward or distribute the text or part of it, without the consent of the author(s) and/or copyright holder(s), unless the work is under an open content license such as Creative Commons.

Takedown policy
Please contact us and provide details if you believe this document breaches copyrights.
We will remove access to the work immediately and investigate your claim.

This work is downloaded from Delft University of Technology.
For technical reasons the number of authors shown on this cover page is limited to a maximum of 10.

sustainability

MDPI

Article

Effect of Activator and Mineral Admixtures on the Autogenous Shrinkage of Alkali-Activated Slag/Fly Ash

Yuwei Ma [1,*], Jihao Gong [1], Guang Ye [1,2] and Jiyang Fu [1,*]

[1] Research Center for Wind Engineering and Engineering Vibration, Guangzhou University, Guangzhou 510006, China; 1111916002@e.gzhu.edu.cn (J.G.); g.ye@tudelft.nl (G.Y.)
[2] Microlab, Section Materials and Environment, Faculty of Civil Engineering and Geosciences, Delft University of Technology, Stevinweg 1, 2628 CN Delft, The Netherlands
* Correspondence: yuwei_ma@gzhu.edu.cn (Y.M.); jiyangfu@gzhu.edu.cn (J.F.)

Abstract: The high autogenous shrinkage of alkali-activated fly ash/slag (AASF) poses a significant concern for the widespread application of AASF in structural engineering. The present study compares the efficacy of activator and mineral admixtures in mitigating the autogenous shrinkage of AASF, and discusses the underlying mechanism. The results show that the use of activators with a lower silicate modulus and a lower sodium content, as well as incorporating metakaolin (MK) or silica fume, can reduce the autogenous shrinkage of AAMs. These approaches delay the appearance of the second exothermic peak, which corresponds to the later formation of C-A-S-H gels and slower development of capillary pressure. The inclusion of MK not only retards the reaction but also facilitates the formation of N-A-S-H gels, resulting in a coarse pore structure and reduced water consumption. The use of the activator with a lower silicate modulus (reduced from 1.5 to 1.0) leads to a higher internal relative humidity and the reduced pore volume of silt-shaped and ink-bottle pores (2–50 nm) in AASF, thereby reducing the autogenous shrinkage without significant strength reduction.

Keywords: alkali-activated fly ash/slag; autogenous shrinkage; capillary pressure; shrinkage mitigation

check for updates

Citation: Ma, Y.; Gong, J.; Ye, G.; Fu, J. Effect of Activator and Mineral Admixtures on the Autogenous Shrinkage of Alkali-Activated Slag/Fly Ash. *Sustainability* **2023**, *15*, 16101. https://doi.org/10.3390/su152216101

Academic Editor: José Ignacio Alvarez

Received: 9 October 2023
Revised: 4 November 2023
Accepted: 16 November 2023
Published: 20 November 2023

Copyright: © 2023 by the authors. Licensee MDPI, Basel, Switzerland. This article is an open access article distributed under the terms and conditions of the Creative Commons Attribution (CC BY) license (https://creativecommons.org/licenses/by/4.0/).

1. Introduction

The production of ordinary Portland cement (OPC) is responsible for approximately 2.9 billion tons of carbon dioxide emissions in 2021, accounting for 7% of global CO_2 emissions [1]. The development of low-carbon binders is thus regarded as of imperative priority. Alkali-activated materials (AAMs), which are prepared by using alkaline activators and industrial by-products, such as ground granulated blast-furnace slag (GGBFS) and fly ash, are recognized as promising alternatives to OPC in view of their low CO_2 emission [2,3], superior mechanical properties [4,5] and durability [6,7]. The improved performance and greater environmental benefits offered by AAMs would contribute to the sustainability of the construction industry. Despite these favorable properties, AAMs suffer from significantly high shrinkage in the early age, particularly when GGBFS is used as the main precursor [8,9]. It has been widely reported that the autogenous shrinkage of alkali-activated blast-furnace slag (AABFS) is 5–7-fold larger than that of OPC with the same water/binder ratio [10,11]. Self-desiccation [12] is generally regarded as the main driving force for autogenous shrinkage in AABFS, in which the internal relative humidity (IRH) drops due to the consumption of water and then leads to the development of capillary pressure.

Parameters related to self-desiccation, e.g., internal relative humidity, pore structure, surface tension, capillary pressure, and the elastic modulus, have been investigated by numerous researchers. Song et al. [13] compared the IRH of AAMs with sodium carbonate and a combination of sodium silicate and sodium hydroxide as activators. They found that the IRH of AAMs prepared by sodium silicate and sodium hydroxide dropped to 82%

at the age of 28 days, which was much lower than that using sodium carbonate as the activator (93%). Another important factor associated with the high shrinkage of AABFS is the higher volume of mesopores (1.25–25 nm) than that in OPC. It is reported that up to 80% of the pores in AABFS paste were mesopores, while only 36.4% of pores in OPC paste were mesopores, with a larger percentage of macropores (25–5000 nm) [14]. The meniscus formation from finer pores results in significantly higher capillary pressure [14]. Chen et al. [15] reported that the autogenous shrinkage of AABFS increased as the silicate modulus increased from 0.5 to 1.0, followed by a reduction as the silicate modulus increased to 1.5 and 2.0. They claimed that excessive silicate in the activator retarded the consumption of internal moisture, and subsequently decreased the autogenous shrinkage. However, Kumarappa et al. [10] found that a higher Na_2O content and a higher silicate modulus led to higher capillary stress and greater autogenous shrinkage. They calculated the autogenous shrinkage of AABFS by using the model proposed by Bentz and the capillary pore pressure model. Their results showed that the measured shrinkage strain was 10-fold larger than the calculated value, indicating other mechanisms affecting the autogenous shrinkage of AABFS except for the "self-desiccation" process. Ye et al. [11] pointed out that the rearrangement and reorganization of the C-A-S-H gels exhibited viscoelastic characteristics, which then resulted in large autogenous shrinkage. Li et al. [16] proposed that creep deformation induced by the pore pressure played an important role in the autogenous shrinkage of AAMs.

In order to improve the volume stability of AAMs, measures were applied to reduce the autogenous shrinkage. Li et al. [9] reported that the addition of 10% of metakaolin reduced the autogenous shrinkage of AABFS pastes by 38% at the age of 7 days. Silica fume was also used to improve the early-age shrinkage of AAMs. Kumarappa et al. [10] found that the incorporation of saturated fine lightweight aggregates was able to reduce the autogenous shrinkage of AABFS mortar by providing extra water from the lightweight aggregates. The use of shrinkage-reducing admixtures, e.g., polypropylene glycol (PEG) [17] and ethylene glycol (EG) [18], was also reported as reducing the surface tension of the solution, while SAP provided extra water to compensate for water consumption during the reaction [19,20], which maintained the relatively high IRH and alleviated the development of capillary stress. Qu and Yu [21] found that the usage of biofilm inhibited the increase in capillary pressure and the decrease in the moisture loss of AAS, which resulted in a more efficient shrinkage-reducing effect than the use of SRA.

Given the above literature, it can be deduced that the autogenous shrinkage of AAMs can be mitigated by adjusting the initial mixture design of AAMs, as well as by using different types of additives and admixtures. These methods mainly aim at reducing/delaying the development of capillary pressure in pores by controlling the IRH or reducing the surface tension of the pore solution. However, their effectiveness in shrinkage reduction has seldom compared. In addition, the alleviation mechanism of autogenous shrinkage of AAMs among different measures has not been fully understood. In view of the aforementioned points, this study reduced the autogenous shrinkage of alkali-activated slag/fly ash (AASF) mixtures from the perspective of the mix proportions. The autogenous shrinkage of alkali-activated slag/fly ash (AASF) prepared with a lower Na_2O content and a lower silicate modulus, as well as silica fume and metakaolin as mineral admixtures, were compared with each other. Parameters that are associated with autogenous shrinkage, e.g., heat evolution, internal relative humidity, development of the capillary pressure, reaction products, and pore structure were subsequently examined. The volume change in AABFS and OPC pastes under saturation conditions are compared to clarify the role of "self-desiccation" in these two systems. Based on the experimental results and theoretical calculation, the mechanisms and driving forces of autogenous shrinkage in AAMs were discussed.

2. Materials and Methods

2.1. Raw Materials

Ground granulated blast-furnace slag (GGBFS), fly ash (FA), sodium silicate solution, and NaOH were used to prepare AASF pastes. FA and GGBFS used in this study were supplied by Shaoguan Steel Factory and Zhongshan Electric Power Plant (Guangdong Province), respectively. Silica fume (SF) and metakaolin (MK) were provided by Borun New Materials Co., Ltd. (Gongyi, China) and Chenyi Materials Co., Ltd. (Gongyi, China) in Henan Province, respectively. The chemical composition of the raw materials characterized by the X-ray fluorescence spectrometer (XRF) is given in Table 1. It can be found that the main components of GGBFS and FA are SiO_2, CaO, and Al_2O_3. Silica fume is mainly composed of SiO_2, and metakaolin has the highest contents of Al_2O_3 among these precursors. The density and surface area (measured by N_2 adsorption) of the raw materials were also presented in Table 1. Figure 1a presents the mean particle size of the raw materials, the MK has the smallest median particle size (d50) of 7.1 µm, while FA has the largest d50 of 18.8 µm. Additionally, GGBFS and SF have d_{50} values of approximately 11.67 µm and 7.96 µm, respectively. Figure 1b shows the crystalline phases of raw materials. Gehlenite ($Ca_2Al_2SiO_7$) is identified in GGBFS, and albite ($NaAlSi_3O_8$), microline ($KAlSi_3O_8$), and quartz (SiO_2) are identified in FA. MK and SF are mainly amorphous. Commercial sodium hydroxide powder (analytical grade, >98% purity) and sodium silicate solution (Na_2O: 12.19 wt.%; SiO_2: 28.18 wt.%, H_2O: 59.63 wt.%) and distilled water were used to produce the activator.

Table 1. Chemical compositions and physical properties of raw materials.

	SiO_2 (%)	Al_2O_3 (%)	Fe_2O_3 (%)	SO_3 (%)	MgO (%)	CaO (%)	K_2O (%)	Na_2O (%)	Others (%)	L.O.I (%)	Density g/cm^3	Specific Surface Area (m^2/g)
GGBFS	34.4	16.9	0.4	2.3	6.2	38.1	0.4	0.2	1.1	−1.5	2.84	0.75
FA	55.0	15.1	6.0	0.7	2.8	13.4	3.8	1.6	1.7	1.5	2.81	1.46
SF	98.3	0.5	0.2	-	0.1	0.1	-	0.1	0.7	-	1.64	20.39
MK	55.06	43.02	0.76	-	0.06	0.17	0.55	0.06	0.32	-	2.65	10.82

L.O.I stands for the loss of ignition.

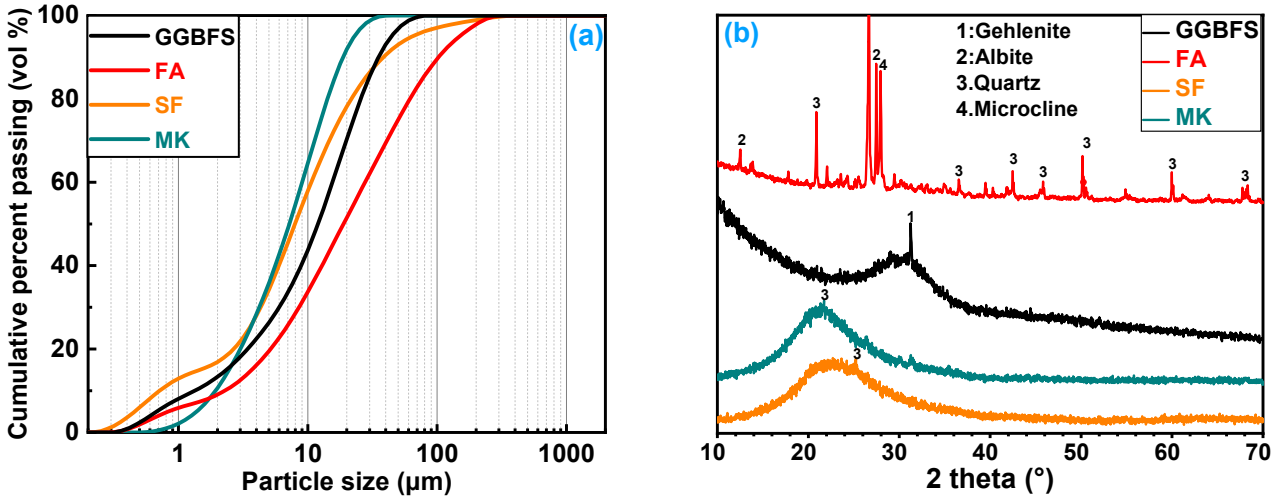

Figure 1. Particle size distribution (**a**,**b**) XRD pattern of raw materials (ground granulated blast-furnace slag (GGBFS), fly ash (FA), Silica fume (SF) and metakaolin (MK)). (Gehlenite: $Ca_2Al_2SiO_7$, albite: $NaAlSi_3O_8$, quartz: SiO_2, and microline: $KAlSi_3O_8$).

2.2. Mixture Design and Sample Preparation

The alkaline activator was prepared by mixing hydroxide powder, sodium silicate solution and distilled water together. All activator solutions were prepared and stored at a

temperature of 20 °C for 24 h before the sample preparation. AASF pastes were prepared at a constant GGBFS/FA weight ratio of 5:5 and a water/binder (GGBFS+FA) ratio of 0.4. The water content from waterglass was also considered in the mixing water. Two different Na_2O dosages (4% and 5%) and silicate moduli (1.5 and 1.0) were applied in this study. These mixtures were chosen from a previous study [22], which exhibited sufficient mechanical strength at the age of 7 days (>40 MPa). Two different mineral admixtures, i.e., silica fume and metakaolin with a weight ratio of 10%, were added to evaluate their effects on the autogenous shrinkage. The samples used for compressive strength were prepared in molds with a dimension of 40 × 40 × 40 mm^3. For the samples that were used for XRD, pore structures, the fresh paste was poured into a plastic bottle and sealed with a lid. Then, all samples were sealed cured in a standard chamber (20 ± 1 °C, relative humidity above 95%) until the desired curing age. Samples were soaked into isopropanol for 3 days to terminate the reaction once they reached the desired curing age. The treated samples were then dried at 60 °C in a vacuum oven until they reached a constant mass. Furthermore, the samples designated for XRD were ground into powders that passed through the 45 μm sieve prior to testing.

Table 2 presents the detailed mixture design for the investigated AASF pastes. For sample preparation, raw materials were preliminarily dry-blended in the mixer for 2 min and the activator solutions were added to the mixer and then mixed for another 3 min. The samples used for compressive strength were prepared in molds with a dimension of 40 × 40 × 40 mm^3. For the samples that were used for XRD, pore structures, the fresh paste was poured into a plastic bottle and sealed with a lid. Then, all samples were sealed cured in a standard chamber (20 ± 1 °C, relative humidity above 95%) until the desired curing age. Samples were soaked into isopropanol for 3 days to terminate the reaction once they reached the desired curing age. The treated samples were then dried at 60 °C in a vacuum oven until they reached a constant mass. Furthermore, the samples designated for XRD were ground into powders that passed through the 45 μm sieve prior to testing.

Table 2. Mix design of AASF pastes.

Samples	GGBFS (g)	FA (g)	MK (g)	SF (g)	Na_2O (g)	SiO_2 (g)	Water to Binder	Modulus (Ms)
Ref	50	50			5	7.26		1.5
N4	50	50			4	5.81		1.5
M1	50	50			4	3.87	0.4	1.0
MK10	50	50	10		4	5.81		1.5
SF10	50	50		10	4	5.81		1.5

2.2.1. Heat Evolution

The heat evolution of AASF pastes was measured by an isothermal calorimeter (TAM-Air-314). All the raw materials were stored at 20 °C for 24 h in advance, and the device was calibrated at the same condition before the experiment. Approximately 10 g (±0.01 g) of fresh AASF paste and corresponding reference water were placed into glass ampoules. Then, the ampoules were carefully put in the calorimeter channel. The whole test preparation was controlled within 5 min. The data of heat evolution were continuously recorded for 168 h. Three samples were replicated in each mixture.

2.2.2. Capillary Pressure

Figure 2 presents the schematic diagram and experimental setup for the capillary pressure measurement system according to a previous study [23]. The measurement system was connected to a ceramic head through a PVC tube. First, the ceramic head, together with the PVC tube, was saturated with water with a pump and then sealed on the top of the system by a cover. The ceramic head has many tiny micropores and can be thought of as a rigid porous layer, which acts as a sensing element in the device. When the ceramic head was immersed in water, the water films were generated in these tiny pores. The

tension in pore water can guarantee water transfer through the ceramic head by pores while restraining the movement of air. As the ceramic head made contact with the AASF pastes, a hydraulic connection was established between the water in the PVC pipe and the water in the pore solution. The pore water in the paste gradually consumes with the process of reaction and then became unsaturated. The water potential gradient between the pipe and pore solution leads to water being transported from the ceramic head into the paste until a new stabilization is reached. The negative pressure was produced in the water pipe with the continuous reaction. The capillary pressure measurement system can measure the pressure ranging from 0 to 100 kPa with an accuracy of 0.25 kPa.

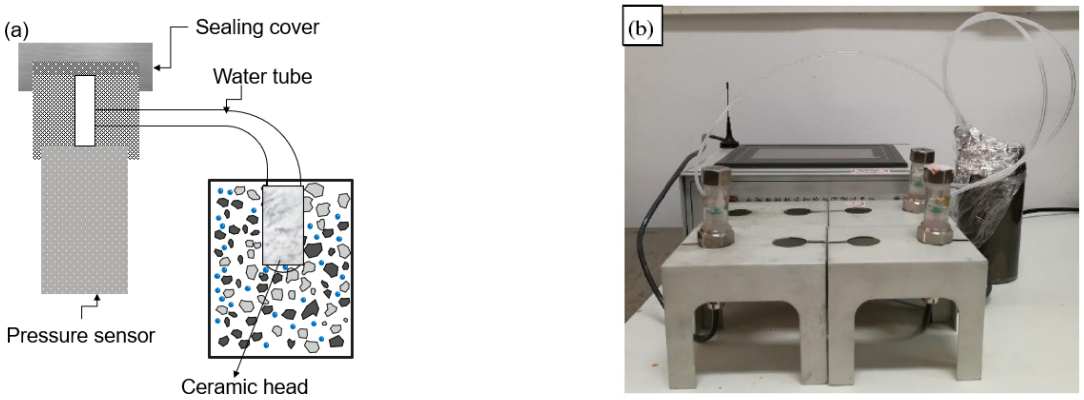

Figure 2. (**a**) The schematic diagram of capillary pressure test setup; (**b**) experimental setup for internal pressure test [23].

2.2.3. Internal Relative Humidity (IRH)

The IRH of AASF pastes was measured by Rotronic HC2-AW RH sensors, which can monitor the IRH of AAMs and OPC from very early ages [24]. Before the experiment, the RH sensors were calibrated by saturated salt solutions (NaCl, KCl, K_2SO_4) with RH in the range of 65–95%. The fresh paste was placed in a PVC container and put in the measuring chamber. The temperature during the measurement was kept constant at 20 ± 0.2 °C. The IRH values of samples were measured at a frequency of 1 min till 7 days. The IRH corresponds to the mean value of two sets of measurements.

2.2.4. Autogenous Shrinkage

The fresh AASF pastes were cast into the corrugated molds with a length of 420 mm and 29 mm in diameter to measure the autogenous shrinkage in accordance with ASTM C1968-09 [25]. This method is suggested to measure the autogenous shrinkage because it prevents moisture loss and minimizes restraint to volume change. After casting, the specimen was immediately sealed with two plugs and sealing glue and horizontally placed on a container with a linear variable differential transformer (LVDT) fixed on one end plate. The test temperature was controlled at 20 ± 0.1 °C by immersing the whole equipment in a thermostat with a silica-oil bath. The length change in the AASF paste was automatically recorded at an interval of 1 min and the test was kept for up to 7 days. Each mixture was set to three replicates to measure.

According to a previous literature [16], a modified corrugated tube method was employed to measure autogenous shrinkage of AASF pastes under two different saturated conditions (water and sodium silicate solution). This method has been proven to be effective in measuring under saturated conditions. The AASF pastes were cast into a corrugated tube that was only 80% volume filled, and then the top-end plug was sealed and the tube was vibrated horizontally. The same procedure as the autogenous shrinkage measurement was followed to measure the pastes under saturation conditions. During the test, the glycerin level surrounding the tubes was kept slightly lower than the top of the tubes. After the final setting of the pastes, three tiny holes were made on the top of the tube along the

length direction using a needle. Subsequently, the liquid (activator or water) was gently introduced into the tube through these holes until it completely submerged the upper surface of the sample.

2.2.5. X-ray Diffraction

The crystalline phases in the AASF pastes were examined by the X-ray diffraction (XRD) test using an Ultra VI diffractometer. Cu-Kα radiation with a wavelength of 1.54 Å was utilized as the energy resources, and tube settings were 40 kV and 40 mA. The data were collected over a range of 10–65° 2θ with a step size of 0.03° and a scan rate of 2°/min.

2.2.6. Pore Structure Characterization

The pore structure, including the porosity and pore size distribution of AASF pastes, were measured by nitrogen adsorption test and mercury intrusion porosimetry (MIP) test, respectively.

The nitrogen adsorption test was carried out by Micromeritics ASAP 2460 analyzer. Approximately 3 g of AASF samples were vacuum dried at 60 °C until the pressure was reached under 10 Pa. Then, the samples were moved to the measuring channel with the relative pressure (P/P_0) ranging from 0.05 to 0.995. The pore size distribution was derived using Barrett–Joyner–Halenda (BJH) mode [15].

MIP measurements were conducted using a Micromertics Autopore V9600 instrument. For the MIP test, samples were cut into a size smaller than 1 cm^3. The analysis was carried out in two stages: the low-pressure stage ranging from 0 to 0.0036 MPa, and the high-pressure stage, from 0.0036 to 210 MPa, followed by an extrusion process from 210 to 0.14 MPa. The contact angle and the surface tension were chosen as 140° and 0.485 N/m, respectively.

2.2.7. Compressive Strength

The compressive strength of AASF was tested according to EN 196-1 [26]. The freshly mixed paste was poured into a mold with 40 × 40 × 40 mm^3. A universal material testing machine (Instron-5984) was used for compressive strength tests with a fixed rate of 2.5 kN/s. For each mixture, at least three replicates were conducted.

3. Results

3.1. Heat Evolution of AASF Pastes

Figure 3 shows the heat evolution of AASF pastes with different activator contents and mineral admixtures. The initial exothermic peak that appeared in the first 1–2 h is ascribed to the initial wetting and dissolution of raw materials [9]. Afterward, all the mixtures showed one main exothermic peak, which is known to correspond to the acceleration period of the reaction, indicating the formation of C-A-S-H gel [16]. It is observed from Figure 3a that AASF mixture with a lower Na_2O content (N4) presented a later appearance of the acceleration period and a lower main exothermic peak intensity. Correspondingly, the cumulative heat release of mixture N4 was lower than that of mixture Ref. This is because a lower alkali concentration reduced the pH of the activator. Less slag and fly as particles dissolved, leading to a lower degree of reaction of sample N4 at 7 days [22,27]. For mixture M1, which had a lower silicate modulus (1.0), the main exothermic peak shifted to a later time, while the cumulative heat release was higher than that of mixture N4 (silicate modulus 1.5). It seems that less SiO_3^{2-} in the activator (lower silicate modulus in this study) decelerated the formation of C-A-S-H gel while promoting the dissolution of slag particles. More Ca, Si, and Al species dissolved from the slag, leading to a higher degree of reaction at 7 days. Similar findings were also reported in previous studies [10,28]. The AASF mixture with silica fume (SF10) and metakaolin (MK10) exhibited even delayed acceleration periods and lower exothermic peak intensity. These two mixtures had lower cumulative heat release at 7 days, indicating a lower degree of reaction. The addition of SF and MK increased the amounts of Si and Al in AASF and consumed alkali for dissolution,

which would result in retarding the subsequent dissolution of slag [29]. It is found that the addition of MK delayed the reaction most significantly, in comparison with other methods, as shown in Figure 3. This agreed with previous literature that increasing the amount of Si and Al in the AABFS system would decrease the formation of C-A-S-H gels [9].

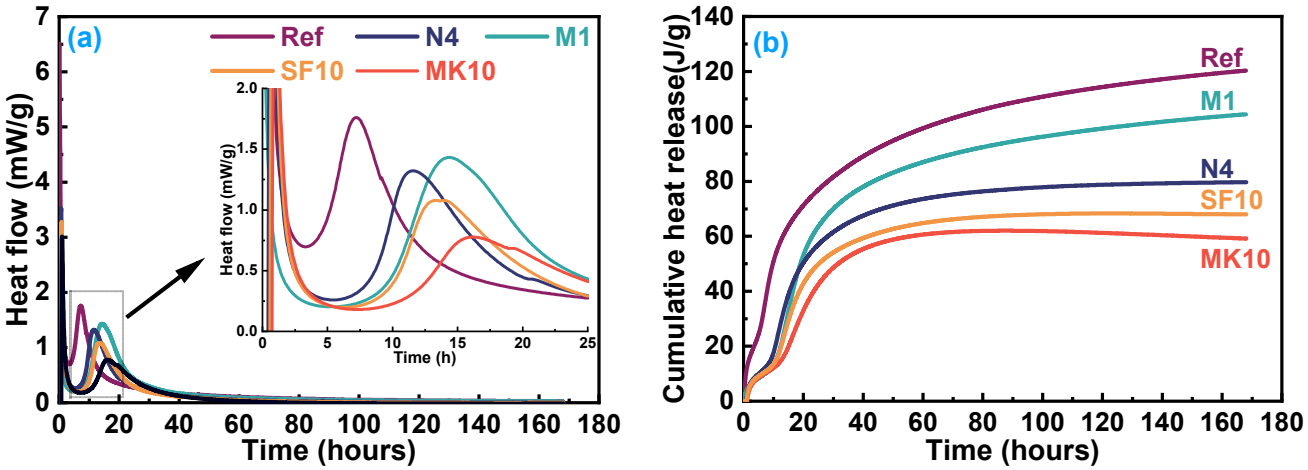

Figure 3. Effect of activators and mineral admixtures on the heat evolution of AASF paste: (**a**) heat flow and (**b**) cumulative heat release.

3.2. Capillary Pressure Development in AASF Pastes

Figure 4 presents the development of the capillary pressure in different AASF mixtures. At the beginning of the reaction, the development of the capillary pressure was slow, then increased promptly after a period of reaction time. This period when capillary pressure suddenly increases (known as "transition time"), corresponding to the formation of the water–air meniscus in pores, is known as the "time-zero" for self-desiccation [23,30]. As noticed in Figure 4, mixture Ref exhibited positive pressure in the initial stage of the reaction. This may be ascribed to the ions entering the ceramic head and moving with water migration when the pH environment was high. To achieve the ion concentration balance in the ceramic head film, positive capillary pressure was formed. The transition time of mixture Ref was set at approximately 1.0 h when the capillary pressure rapidly increased, as shown in Figure 4. The use of an activator with a lower sodium content (N4) and a lower silicate modulus (M1), together with the addition of SF (SF10) and MK (MK10), prolonged the appearance of transition time. For example, the transition time of AASF pastes increased from approximately 1.0 h to 6.6 h as the Na_2O content changed from 5% to 4%. The addition of MK and a reduced silicate modulus from 1.5 to 1.0 prolonged the transition time more effectively than the use of SF. The delayed transition time revealed a decelerated development of capillary pressure in the AASF system. This is in line with the heat release results: mixtures exhibited delayed exothermic peaks and had slower development of capillary pressure. It is well known that the appearance of the main exothermic is associated with the formation of C-A-S-H gel, in which reaction water is consumed and becomes chemically bonded. The consumption of water leads to the formation of water–air meniscus and the development of capillary pressure. It is derived that the development of capillary pressure is directly related to the formation of C-A-S-H gels. Decreasing the amount of SiO_3^{2-} in the activator or using MK are effective measures to delay pressure development.

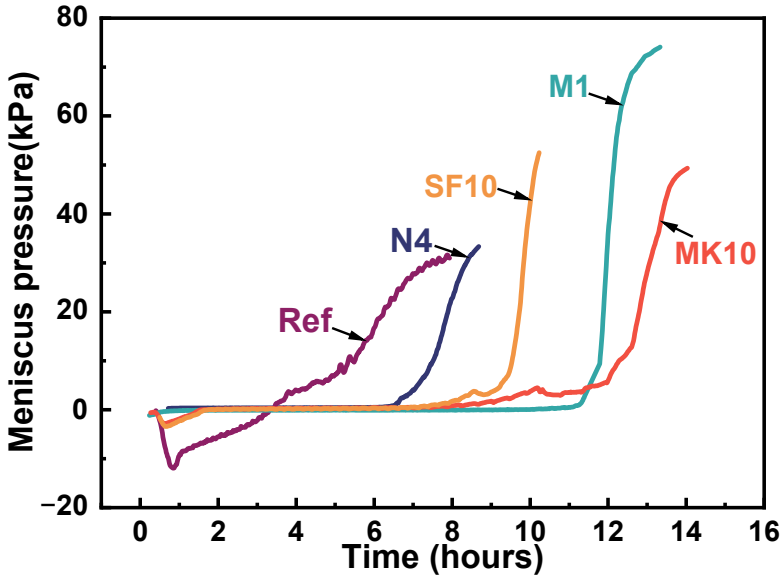

Figure 4. The development of capillary pressure of different AASF mixtures.

3.3. Internal Relative Humidity of AASF Pastes

The development of IRH of AASF pastes with different activators contents and mineral admixtures in the early age is illustrated in Figure 5. The measured IRH of all samples increased rapidly in the first 1–2 h, which was caused by the moisture equilibration between the RH sensor and the specimens. Afterwards, a decline of IRH occurred in most AASF mixtures except for MK10. The reduction in IRH in mixture Ref, with an Na_2O content of 5% and a silicate modulus of 1.5, was the most dramatic: the 7-day IRH decreased from 96.54% to 72.96%, as shown in Figure 5. The high Na_2O content provides a higher pH condition, resulting in the extensive dissolution of slag particles [10]. Therefore, the concentrations of ions, such as Al, Si and Na, in the mixture Ref are higher than in other mixtures. It is reported in a previous study [15] that the surface tension was higher for activators with a higher Na_2O and silicate content. Hence, the drop of IRH in the mixture Ref was the fastest. This was in line with the findings by Chen et al. [15], who reported that the IRH of AAS pastes declined from approximately 72.5% to 60% as the alkalinity increased from 4% to 6%.

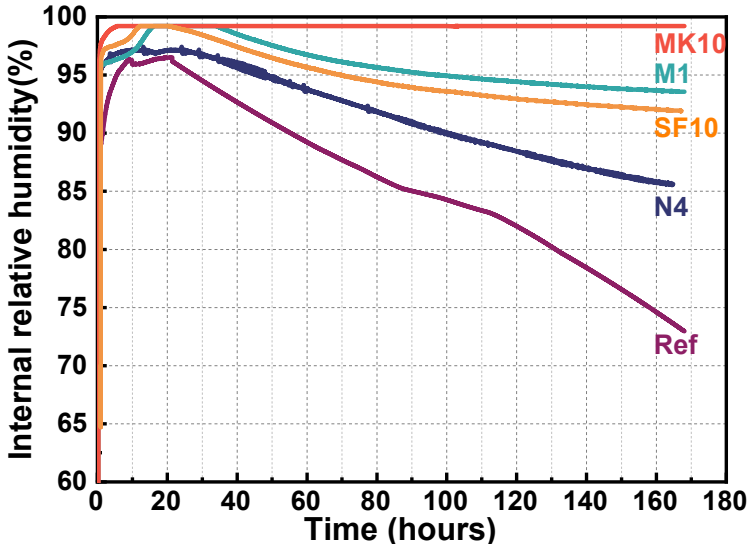

Figure 5. Effect of different factors on the internal relative humidity of AASF pastes.

AASF with a lower Na_2O content (N4) displayed a slower IRH drop than the mixture Ref, followed by SF10 and M1. For AASF with metakaolin (MK10), the IRH remained at a very high value during the first 7 days. In general, both the results from the IRH and capillary pressure measurements showed the same trend: the addition of MK and the use of an activator with a lower silicate modulus can effectively alleviate the drop of IRH and capillary pressure development. However, the IRH may not provide the actual values of the capillary pressure at the early age, especially for the samples with high IRH. On the other hand, the measurement of capillary pressure is generated more intuitively and accurately, corresponding to the "time-zero" of self-desiccation from its physical definition.

3.4. Autogenous Shrinkage of AASF Pastes

Figure 6 shows the autogenous shrinkage of all investigated AASF pastes in the first 7 days, as measured by means of the corrugated tube method. The "time-zero" of autogenous shrinkage was set as the time that capillary pressure rapidly raised. Similar to the trend of IRH, AASF mixtures with lower IRH presented a higher magnitude of autogenous shrinkage. Mixture Ref, with a higher Na_2O content and a higher silicate modulus, exhibited the largest autogenous shrinkage, i.e., approximately 6896 με at the age of 7 days, which was consistent with the results as reported by Chen et al. [15]. This value was significantly larger than that of OPC pastes, of which the autogenous shrinkage was lower than 1000 με. Mixture N4 showed a lower autogenous shrinkage than mixture Ref, followed by mixture SF10 (5124 με) and mixture M1 (4563 με). It seems that the lower amount of SiO_3^{2-} ions supplied by the activator decelerated the development of capillary pressure and the rate of IRH drop. Consequently, mixture M1 exhibited a lower autogenous shrinkage than mixture N4. The addition of MK prominently reduced the autogenous shrinkage of AASF to 1911 με at 7 days (a reduction of approximately 68.9%). Similar findings were also reported in the literature [9], where the addition of 10% MK in AABFS decreased the autogenous strain from 6900 με to approximately 4000 με. It is reported that the dissolution of MK reduced the concentration of Na^+ and OH^- ions in the pore solution and provided additional dissolvable Si and Al for the system [9]. Therefore, the reaction rate and generation of C-A-S-H gels in AASF pastes were slowed, resulting in a lower autogenous shrinkage [31].

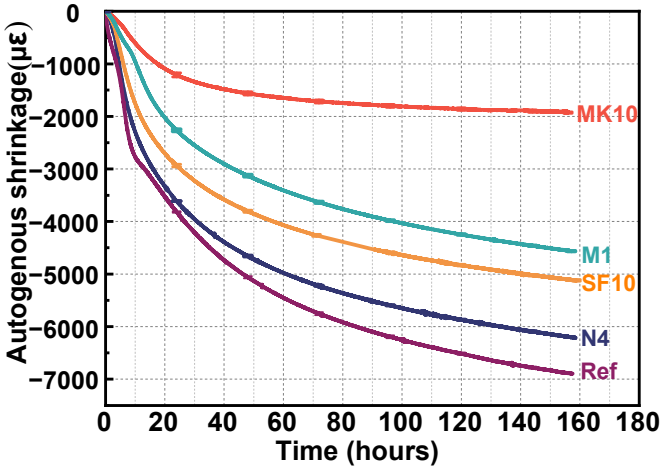

Figure 6. Autogenous shrinkage of AASF pastes with different activators and mineral admixtures.

3.5. XRD Analysis

Figure 7 displays the XRD diffractograms of all investigated mixtures at the age of 1 day and 7 days. The crystalline phase identified includes albite and microline originating from unreacted fly ash. In accordance with previous research [9], the XRD pattern of all AASF samples presented a broad diffraction peak at 2θ of approximately 29.2°–29.8°, corresponding to the formation of C-A-S-H gels. As illustrated in Figure 7a, the peak

intensity at 29.2° in AASF mixtures (except MK10) was related to the formation of C-A-S-H-type gels [3]. Meanwhile, the broad diffraction bump shifted to a higher 2θ at approximately 30° for mixture MK10, indicating the formation of another type of amorphous phase, namely sodium aluminum silicate hydrate (N-A-S-H) gels [9,32]. Bernal [29] and Li [9] reported that the addition of MK in AABFS would favor the formation of N-A-S-H gels or zeolite phased when calcium was not largely available at the early age. The dissolution of MK released additional Si and Al to the pore solution and promoted the formation of N-A-S-H gels. The XRD patterns of all investigated AASF mixtures showed no obvious changes in the main reaction products at 1 day and 7 days (except the MK10 mixture), suggesting that the reduction in autogenous shrinkage of AASF pastes is not related to different types of reaction products, but rather to the amount of reaction products.

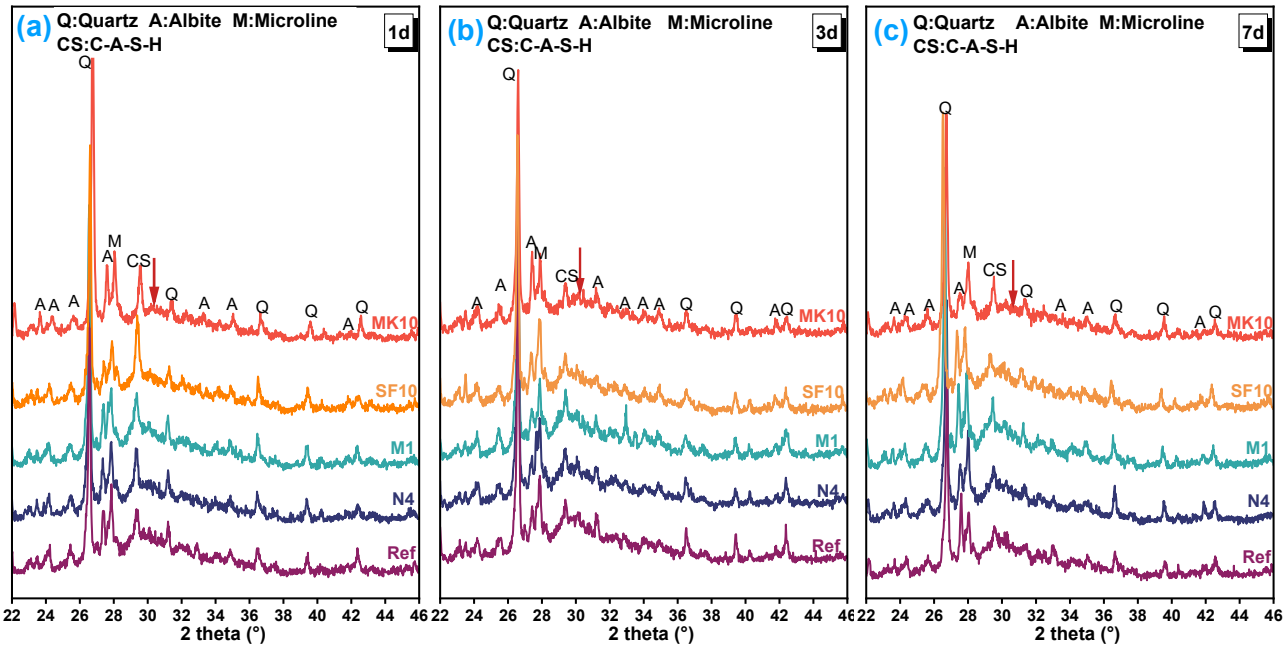

Figure 7. XRD patterns of AASF pastes cured for (**a**) 1 day, (**b**) 3 days, and (**c**) 7 days. (Quartz: SiO_2, albite: $NaAlSi_3O_8$, and microline: $KAlSi_3O_8$).

3.6. The Pore Structure of AASF Pastes

Figure 8 illustrates the pore size distribution and differential curves (derived from the MIP tests) of AASF pastes prepared with different activator contents and MK, SF addition at the age of 7 days. The MIP test can determine a wide range of pore sizes (from 0.005 μm to 800 μm in this study) that are needed for pore structure characterization of cementitious materials. It is observed from Figure 8a that mixture Ref had the smallest total porosity (14.7%) at 7 days, revealing the formation of a dense microstructure. A reduction in sodium content (mixture N4) led to a significantly higher total porosity (24.06%) in comparison with mixture Ref. This is associated with a lower degree of reaction of mixture N4 than that of mixture Ref. Mixture M1 and SF10 presented lower total porosity at approximately 18.8% than mixture N4. Compared to mixture N4, mixture M1 had lower SiO_2 content in the activator, implying that extra silicate ions provided by the activator inhibited the further reaction of slag, and led to a higher total porosity. Although mixture SF10 had a lower degree of reaction than mixture N4, the silica fume filled the pores of AASF, leading to a lower total porosity. On the other hand, mixture MK10 exhibited the largest total porosity (35.47%) compared with other AASF mixtures. Following the intrusion process, extrusion of mercury was employed to assess the pore connectivity in AASF. The volume of mercury retained during extrusion process is defined as "ink-bottle" porosity, while subtracting this value from total porosity is defined as "effective porosity". It is evident that mixture MK10

had the greatest effective porosity than the other mixtures, indicating the well connectivity of the pores.

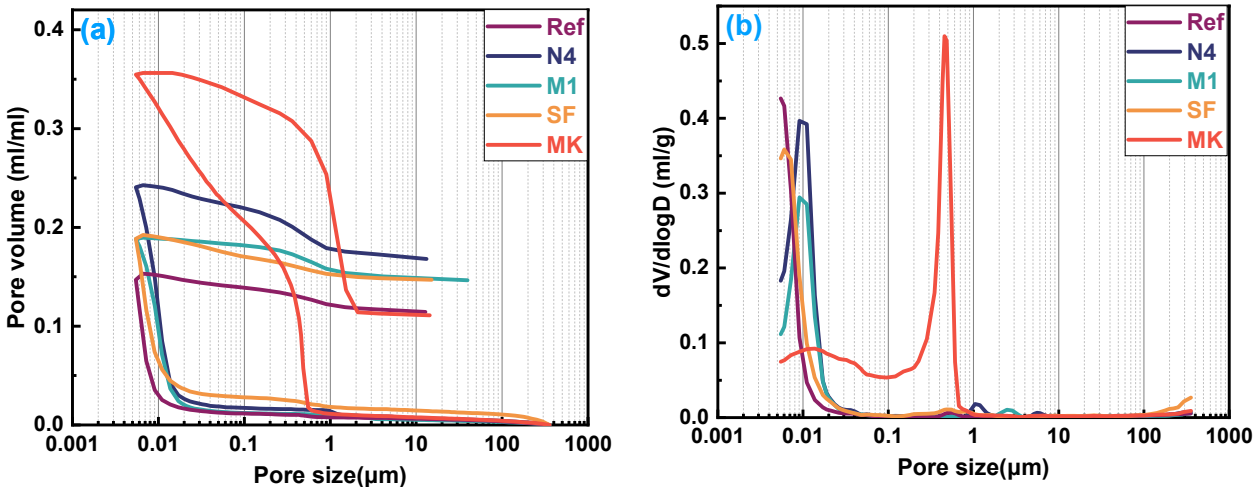

Figure 8. MIP results of all samples at 7 days: (**a**) pore volume and (**b**) pore size distribution.

From its pore size distribution curves, as shown in Figure 8b, it is found that except for the gel pores, a distinct peak at the pore diameter of 0.5 μm was observed in MK10, while such a peak was not detected in other AASF mixtures. The differential curves of other AASF mixtures exhibited only one peak corresponding to the gel pores, with a pore diameter at approximately 10 nm. The coarser pore structure of AASF, when slag was substituted by metakaolin, was consistent with the findings from previous literature [9]. The introduction of MK into the system promoted the transformation of the gel phase from C-A-S-H gel into N-A-S-H gel, which had a poorer space-filling capacity than C-A-S-H gel [33]. As a result, a distinct peak at 0.5 μm was present in mixture MK10, which was also related to the lower degree of reaction of AASF when MK was added. The other four AASF mixtures displayed similar pore size distribution, implying the formation of the same type of gel phase of AASF with different activator content and silica fume addition. Compared with MIP measurement, nitrogen adsorption/desorption measurement provides more detailed information on the gel pores and can detect pores between 2 nm to 100 nm. Figure 9. presents the nitrogen adsorption and desorption curves of AASF paste at the age of 1 day, 3 days and 7 days.

According to the International Union of Pure and Applied Chemistry (IUPAC) classification [34], the adsorption and desorption isotherm of the investigated AASF mixtures can be categorized as type IV, of which most of the pores in AASF mixtures are in the range of 2 nm–50 nm [35]. The AASF mixture with a higher nitrogen-adsorbed quantity indicates a higher pore volume of mesopores, as seen in Figure 10a. AASF mixtures with increased Na_2O and SiO_2 content, i.e., Ref, had higher adsorption quantities, indicating a higher volume of mesopores. Mixture M1, with a lower SiO_2 content (silicate modulus), exhibited the smallest nitrogen adsorption quantity. From the heat release results, it was found that the degree of reaction of mixture M1 was higher than that of mixture N4 and SF10. It implies that extra silicates, either from the activator or from solid materials, increased the volume of mesopores in AASF, which may substantially affect the magnitude of autogenous shrinkage. It was also noticed that mixture MK had the largest nitrogen adsorption quantity at 1 day, while the adsorption quantity decreased with the continuous reaction. The high adsorption quantity is likely induced by the use of MK in AASF, which has a high surface area in the first place. As the reaction proceeded, MK dissolved and reacted to form N-A-S-H gels, leading to reduced mesopores volume. The adsorption/desorption isotherm can also be further used to analyze the hysteresis behavior, which provides important information for the pore shape of materials. Hysteresis loops can be divided into five types based on the IUPAC classification [34]. The isotherms of the AASF mixture at the early age

(1 day) belong to type H1, for which a distinct hysteresis loop exists at P/P_0 of 0.45–1.0 and an inflection point at P/P_0 of 0.5, implying the presentence of silt-shaped pores and some ink-bottle pores. With the continued reaction, the hysteresis loop became wide and the inflection point became sharp, indicating the formation of more ink-bottle pores with relatively narrow pore "neck" and partially blocked pores formed in AASF system. The connectivity of pores in AASF mixtures was reduced, which may also affect the shrinkage strain at the early age. An increase in the sodium and silicate content in the activator generally resulted in an increased nitrogen absorbed amount and hysteresis loop surface, while the use of SF and MK reduced the hysteresis loop surface.

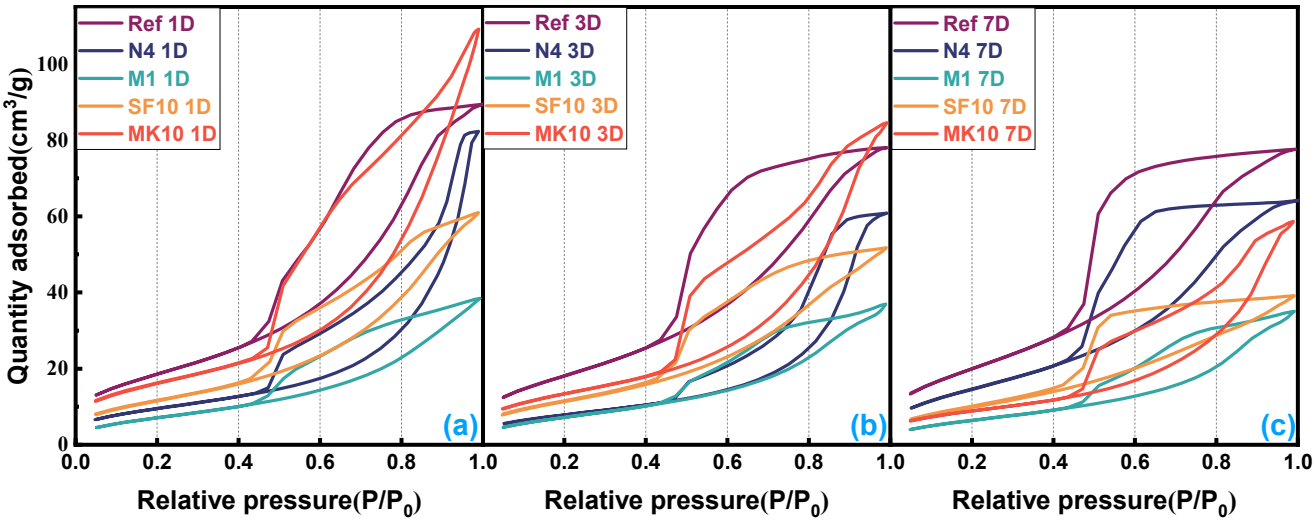

Figure 9. Nitrogen adsorption and desorption isotherms of AASF pastes with different strategies at (**a**) 1 day, (**b**) 3 days, and (**c**) 7 days.

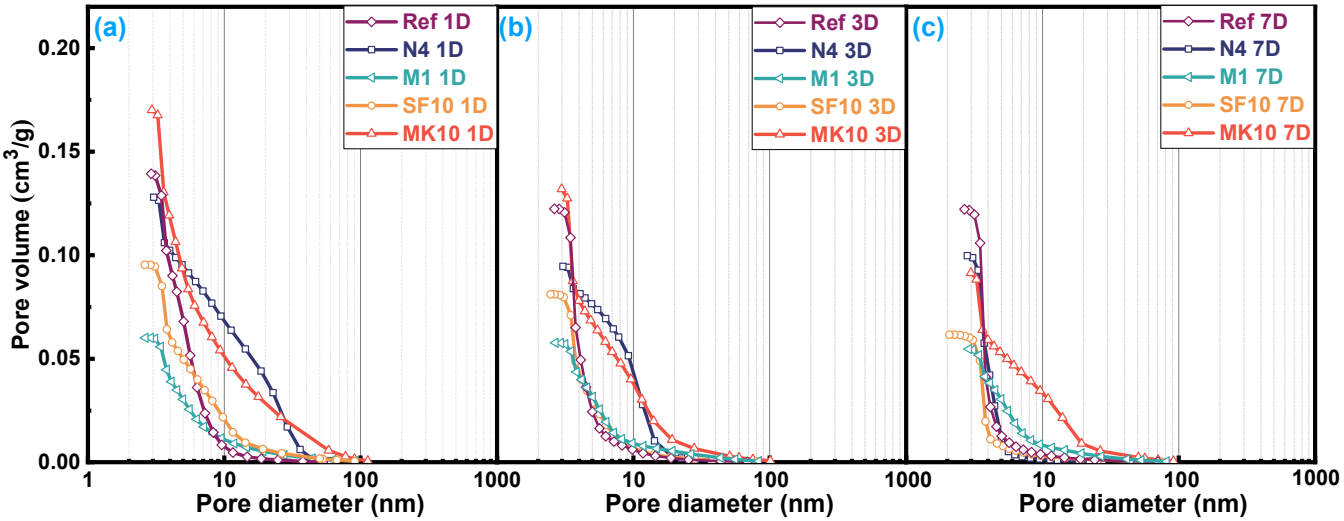

Figure 10. Effect of activators and mineral admixtures on the pore volume of AASF pastes at (**a**) 1 day, (**b**) 3 days, and (**c**) 7 days.

3.7. Compressive Strength

Figure 11 presents the compressive strength of AASF prepared with different activators and mineral admixtures. It is observed that AASF pastes with a higher Na_2O and SiO_2 content (mixture Ref) had the greatest compressive strength, followed by mixture N4 and M1. This is consistent with the findings from previous literature [15,36]. Although mixture M1 had a higher degree of reaction than mixture N4, evidenced by the higher heat release

at 7 days, the compressive strength was still lower. The extra silicate species (provided by the activator) were incorporated into the C-A-S-H gels, leading to a denser microstructure and higher strength. However, the use of mineral admixtures in AASF pastes, e.g., SF and MK, exhibited a negative effect on compressive strength due to a reduction in the degree of reaction, especially at early ages.

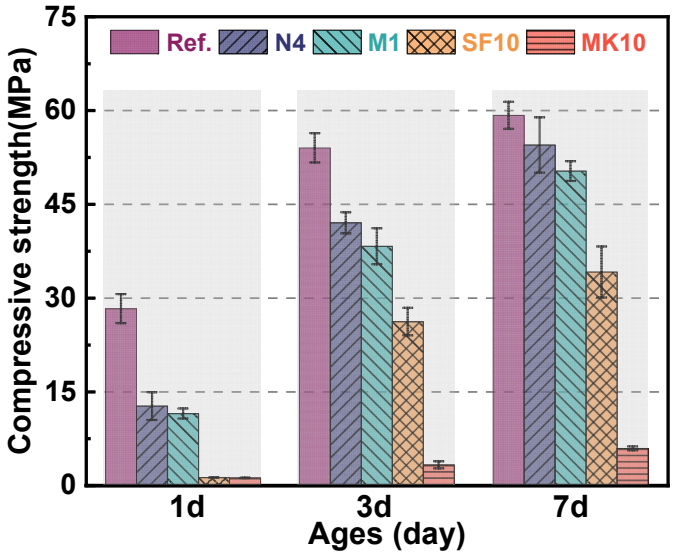

Figure 11. Compressive strength of AASF pastes with different activators (N4, M1) and mineral admixtures (SF and MK) at the early ages.

The significant drop in strength for MK10 was different from the results reported by Li et al. [9], in which the use of 10% and 20% of MK did not dramatically reduce the compressive strength of AABFS pastes. However, in their study, the activator had much higher Na_2O content (9%) than that used in this study (4%). As discussed in Section 3.1, the addition of MK led to a lower degree of reaction of AASF pastes. On the other hand, it can be seen that the MK10 exhibited the largest total porosity among all AASF mixtures. This is attributed to the dissolution of MK releasing additional Si and Al to the system which would favor the formation of N-A-S-H gels, and lead to the coarsening of the pore structure [9,37]. As a result, the compressive strength of the MK mixture was the lowest among all mixtures. In detail, the compressive strength of mixture MK dramatically decreased to 1.16 MPa at 1 day and did not exceed 10 MPa at 7 days. This is in line with some other studies. For instance, Fu et al. [38] reported that the addition of 20% MK in the alkali-activated materials only reached less than 1 MPa before 7 days in an ambient curing condition. Ayeni et al. [39] also reported that the MK-based alkali-activated materials only reached 1.97 MPa at 7 days while the Na_2O dosage was 8 M. The insufficiency of alkali content led to a lower degree of reaction and lower compressive strength as found in Figure 11. From the perspective of strength development and shrinkage control for AASF, the application of an activator with moderate silicate content is recommended for the mixture design of AASF.

4. Discussion

In both cement-based materials and AABFS, the capillary pressure has been widely acknowledged as the main driving force for autogenous shrinkage. Samples with a higher capillary pressure show a larger magnitude of autogenous shrinkage. The generation of capillary pressure is associated with the IRH, which is also related to the reaction kinetics of AAMs. As revealed in Figure 3b, it is evident that AASF mixtures with slower reaction rates, characterized by the late appearance of the main exothermic peak, showed slower development of the capillary pressure correspondingly (Figure 4). The main exothermic peak represented the formation of C-A-S-H gel at the early age. As the reaction proceed, reaction products formed and consumed water and ions in the pore solution. This process

led to a drop in IRH and the formation of small pores. The consumption of water in pores gives rise to the water–air menisci in pores, which leads to the development of tension in the pore solution and contraction of the solid phase (shrinkage). In this study, the use of activators with a lower sodium content and a lower silicate modulus, and the application of MK and SF, were found to delay the formation of reaction products at the early stage, though their mechanism and alleviating effects are different. The XRD results manifest that the main reaction products are C-A-S-H gels, while for mixture MK with metakaolin, N-A-S-H gel was identified. The use of a lower sodium dosage decreased the pH environment in the pore solution and decelerated the dissolution of slag and fly ash grains. This led to a lower degree of reaction of AASF (Figure 3) and less water was chemically bonded into the gel phase. Thus, the decrease in sodium dosage from 5% to 4% led to a reduction in autogenous shrinkage of approximately 780 με in this study, whereas Chen et al. [15] reported that the autogenous shrinkage of AAMs reduced from approximately 6900 με to 5000 με as Na_2O dosage decreasing from 6% to 4%. A decrease in the silicate modulus from 1.5 (N4) to 1.0 (M1) delayed the early formation of the C-A-S-H gel (Figure 3a). However, the degree of cumulative reaction in the M1 system was higher than N4 (Figure 3b). This is in line with the findings in the literature [28]. The addition of excessive silicate species hindered the further dissolution of slag grains. On the other hand, the added silicate could directly react with the Ca and Al species to form C-A-S-H gel, facilitating the formation of gels and water consumption. Therefore, despite the reaction degree in mixture N4 being higher than that of mixture M1, the development of capillary pressure was still delayed. Consequently, the autogenous shrinkage of mixture M1 dramatically decreased by approximately 26% as compared to mixture N4. Similar results were found in other studies [10]. They proposed that the use of sodium silicate with a lower modulus led to a lower surface tension of the pore solutions and thus reduced capillary force. The dissolution of the mineral admixtures, i.e., SF and MK, consumed Na^+ and OH^- ions in the pore solution. Li et al. [9] measured the concentration of Na^+, Ca^{2+}, OH^-, and other ions in the pore solution for alkali-activated slag and alkali-activated slag/MK. They found a significant reduction in the ion concentration for AABFS with the addition of MK. The consumption of OH^- lowered the pH and retarded the dissolution of slag. Therefore, the addition of SF and MK reduced the degree of reaction of AASF, leading to a slower development of capillary pressure. The dissolution of SF released additional Si species into the pore solution, while MK produced Si and Al species. When the concentration of Ca^{2+} in the system was not high, the existence of Na, Si, and Al species would react to form N-A-S-H gel, as revealed by Bernal et al. [29] and Li et al. [9]. It was reported that the formation of N-A-S-H did not consume water. In fact, according to the reaction kinetics, water would be expelled from the gel during the condensation reaction, which kept the IRH at a very high level, as shown in Figure 5. Thus, the addition of metakaolin forms N-A-S-H at the early age, compensating for water consumption caused by the C-A-S-H formation and significantly reducing capillary pore pressure in comparison with the other AASF mixtures. As a result, the addition of 10% MK significantly mitigated the development of autogenous shrinkage of AASF mixtures (a reduction from 6896 με to 1911 με). This is in line with the previous studies. Li et al. [9] reported that the autogenous shrinkage was reduced by 38% and 50% at 7 days, respectively, with the MK content of 10% and 20%, respectively.

The pore structure is another important factor related to the magnitude of autogenous shrinkage. According to the "self-desiccation" theory, water was first emptied into larger pores and then into smaller pores. If water is not sufficient, water–air menisci are formed in pores. According to Kelvin's equation, the largest pore filled with water can be calculated in Equation (1). The capillary stress can be calculated by Kelvin's equation, as

$$ln(RH_k) = \frac{2\gamma V_W}{rRT} \quad (1)$$

where RH_k is the relative humidity due to the menisci formation; γ (N/m) stands for the surface tension and V_w (cm^3/mol) stands for the molar volume of pore solution (18 cm^3/mol), r (m) is the radius of the menisci, R is a constant value for the gas approximately 8.314 (J/(mol·K)). T (K) is the absolute temperature of approximately 293.15 K [16]. According to Kelvin's eqution, water loss from small pores induced much higher capillary stress than that from large pores. That means samples with a larger volume fraction of smaller pores (mesopores) would generate higher capillary stress. As found in this study, the decrease in sodium and silicate content in the activator, as well as the application of SF and MK, led to higher total porosity and coarser pore size distribution of AASF. AASF with 10% of MK, presented another characteristic pore in the range of 0.5 μm, thus having the smallest capillary pressure.

In view of the discussion above, it seems that the high capillary pressure of AASF (mixture Ref and N4) is related to the fast formation of C-A-S-H gels and finer pore size distribution of the matrix, which is closely related to the formation of gel phases. The most important and effective strategy to mitigate the autogenous shrinkage of AASF is to control the formation of C-A-S-H gels at the early age and coarsen the pore structure. In this study, the use of an activator with a lower sodium dosage and a lower silicate modulus, the addition of SF and MK, delayed and reduced the formation of C-A-S-H gels and led to a coarser pore structure. In AASF with MK added, other types of reaction products, i.e., N-A-S-H gels, were formed at the early age. These methods all lead to a lower amplitude of autogenous shrinkage. But the side-effect is clear, i.e., the reduction in compressive strength at the early age. Special attention is needed when conducting the mixture design for AAMs.

5. Conclusions

The effects of the alkali content and the silicate modulus of activators and mineral admixtures (MK, SF) on the autogenous shrinkage of AASF pastes were evaluated and compared in this study. The development of parameters related to autogenous shrinkage as examined, i.e., heat evolution, IRH, capillary pressure, phase composition and pore structure. The detailed conclusions are as follows:

(1) The application of activator with a lower Na_2O content and a lower silicate modulus, as well as the use of silica fume and metakaolin, can reduce the autogenous shrinkage of AASF mixtures. The use of an activator with a reduced silicate modulus and the addition of MK exhibited a more pronounced shrinkage-mitigation effect among the other mixtures. These methods delayed the appearance of the second exothermic peak (later formation of C-A-S-H gels), and slowed down the development of capillary pressure, and IRH drop, corresponding to lower autogenous shrinkage.

(2) The use of MK in AASF led to the formation of N-A-S-H gel at the early age, which compensated for water consumption caused by C-A-S-H gel. Additionally, a distinct capillary pore peak at 0.5 μm was present for mixture MK10 due to the poorer space-filling capacity of N-A-S-H gel and lower degree of reaction. The autogenous shrinkage of mixture MK10 was dramatically reduced, together with its compressive strength.

(3) The increase in Ms from 1.0 to 1.5 deaccelerated the dissolution and reaction of slag. However, the added silicate species acted as reactants and were incorporated into the reaction products, leading to a drop of IRH and an increase in the volume of silt-shaped and ink-bottle pores (2–50 nm) in AASF. The autogenous shrinkage of mixture M1 was dramatically decreased, without significant strength reduction.

It is important to note that in this study, only one type of GGBFS, fly ash, silica fume, and metakaolin, was applied for the investigation. The content of the activator, i.e., sodium silicate, was controlled at a specific range, i.e., sodium content at 4% and 5%, with a silicate modulus between 1.0 and 1.5. This is based on our previous research and previous studies the from the literature. The application of other types of raw materials, as well as other types of activators with different sodium silicate content, may result in different autogenous

shrinkage and microstructure characteristics. Due to the high surface area of metakaolin, it is noted that the sodium content may be insufficient for MK mixtures. However, the application of activator with a higher sodium content and a high w/c ratio may induce other problems (e.g., carbonation and efflorescence) and may not be environmentally beneficial. Therefore, the sodium content in this study was controlled at a relatively low content.

Author Contributions: Conceptualization, Y.M.; Investigation, J.G.; Writing—original draft, Y.M. and J.G.; Writing—review & editing, Y.M. and G.Y.; Supervision, J.F.; Project administration, J.F. All authors have read and agreed to the published version of the manuscript.

Funding: The authors sincerely appreciate the financial supported from the National Natural Science Foundation of China (No.52078149, 52378227), the China National Science Fund for Distinguished Young Scholars (No.51925802), the Bureau of Education of Guangzhou (Grant number: SL2022A03J00938, 202255464) and 111 Project (No. D21021).

Institutional Review Board Statement: This study does not require ethical approval.

Informed Consent Statement: Not applicable.

Data Availability Statement: Data are contained within the article.

Conflicts of Interest: The authors declare no conflict of interest.

References

1. Supriya; Chaudhury, R.; Sharma, U.; Thapliyal, P.C.; Singh, L.P. Low-CO_2 emission strategies to achieve net zero target in cement sector. *J. Clean. Prod.* **2023**, *417*, 137466. [CrossRef]
2. Provis, J.L. Alkali-activated materials. *Cem. Concr. Res.* **2018**, *114*, 40–48. [CrossRef]
3. Ben Haha, M.; Le Saout, G.; Winnefeld, F.; Lothenbach, B. Influence of activator type on hydration kinetics, hydrate assemblage and microstructural development of alkali activated blast-furnace slags. *Cem. Concr. Res.* **2011**, *41*, 301–310. [CrossRef]
4. Duxson, P.; Provis, J.L.; Lukey, G.C.; van Deventer, J.S.J. The role of inorganic polymer technology in the development of 'green concrete'. *Cem. Concr. Res.* **2007**, *37*, 1590–1597. [CrossRef]
5. Provis, J.L.; Palomo, A.; Shi, C. Advances in understanding alkali-activated materials. *Cem. Concr. Res.* **2015**, *78*, 110–125. [CrossRef]
6. Provis, J.L.; Myers, R.J.; White, C.E.; Rose, V.; van Deventer, J.S.J. X-ray microtomography shows pore structure and tortuosity in alkali-activated binders. *Cem. Concr. Res.* **2012**, *42*, 855–864. [CrossRef]
7. Wang, A.G.; Zheng, Y.; Zhang, Z.H.; Liu, K.W.; Li, Y.; Shi, L.; Sun, D.S. The Durability of Alkali-Activated Materials in Comparison with Ordinary Portland Cements and Concretes: A Review. *Engineering* **2020**, *6*, 695–706. [CrossRef]
8. Shi, C.; Qu, B.; Provis, J.L. Recent progress in low-carbon binders. *Cem. Concr. Res.* **2019**, *122*, 227–250. [CrossRef]
9. Li, Z.; Nedeljković, M.; Chen, B.; Ye, G. Mitigating the autogenous shrinkage of alkali-activated slag by metakaolin. *Cem. Concr. Res.* **2019**, *122*, 30–41. [CrossRef]
10. Ballekere Kumarappa, D.; Peethamparan, S.; Ngami, M. Autogenous shrinkage of alkali activated slag mortars: Basic mechanisms and mitigation methods. *Cem. Concr. Res.* **2018**, *109*, 1–9. [CrossRef]
11. Ye, H.; Radlińska, A. Shrinkage mechanisms of alkali-activated slag. *Cem. Concr. Res.* **2016**, *88*, 126–135. [CrossRef]
12. Lura, P.; Jensen, O.M.; Van Breugel, K. Autogenous shrinkage in high-performance cement paste: An evaluation of basic mechanisms. *Cem. Concr. Res.* **2003**, *33*, 223–232. [CrossRef]
13. Song, C.; Choi, Y.C.; Choi, S. Effect of internal curing by superabsorbent polymers—Internal relative humidity and autogenous shrinkage of alkali-activated slag mortars. *Constr. Build. Mater.* **2016**, *123*, 198–206. [CrossRef]
14. Collins, F.; Sanjayan, J.G. Effect of pore size distribution on drying shrinking of alkali-activated slag concrete. *Cem. Concr. Res.* **2000**, *30*, 1401–1406. [CrossRef]
15. Chen, W.; Li, B.; Wang, J.; Thom, N. Effects of alkali dosage and silicate modulus on autogenous shrinkage of alkali-activated slag cement paste. *Cem. Concr. Res.* **2021**, *141*, 106322. [CrossRef]
16. Li, Z.; Lu, T.; Liang, X.; Dong, H.; Ye, G. Mechanisms of autogenous shrinkage of alkali-activated slag and fly ash pastes. *Cem. Concr. Res.* **2020**, *135*, 106107. [CrossRef]
17. Ye, H.; Fu, C.; Lei, A. Mitigating shrinkage of alkali-activated slag by polypropylene glycol with different molecular weights. *Constr. Build. Mater.* **2020**, *245*, 118478. [CrossRef]
18. Bilek, V.; Kalina, L.; Novotny, R. Polyethylene glycol molecular weight as an important parameter affecting drying shrinkage and hydration of alkali-activated slag mortars and pastes. *Constr. Build. Mater.* **2018**, *166*, 564–571. [CrossRef]
19. Tu, W.; Zhu, Y.; Fang, G.; Wang, X.; Zhang, M. Internal curing of alkali-activated fly ash-slag pastes using superabsorbent polymer. *Cem. Concr. Res.* **2019**, *116*, 179–190. [CrossRef]
20. Jiang, D.; Li, X.; Lv, Y.; Li, C.; Jiang, W.; Liu, Z.; Xu, J.; Zhou, Y.; Dan, J. Autogenous shrinkage and hydration property of alkali activated slag pastes containing superabsorbent polymer. *Cem. Concr. Res.* **2021**, *149*, 106581. [CrossRef]

21. Qu, Z.Y.; Yu, Q.; Ji, Y.D.; Gauvin, F.; Voets, I.K. Mitigating shrinkage of alkali activated slag with biofilm. *Cem. Concr. Res.* **2020**, *138*, 106234. [CrossRef]
22. Hu, X.; Shi, C.; Shi, Z.; Zhang, L. Compressive strength, pore structure and chloride transport properties of alkali-activated slag/fly ash mortars. *Cem. Concr. Compos.* **2019**, *104*, 103392. [CrossRef]
23. Ma, Y.; Yang, X.; Hu, J.; Zhang, Z.; Wang, H. Accurate determination of the "time-zero" of autogenous shrinkage in alkali-activated fly ash/slag system. *Compos. Part B Eng.* **2019**, *177*, 107367. [CrossRef]
24. Hu, Z.; Wyrzykowski, M.; Lura, P. Estimation of reaction kinetics of geopolymers at early ages. *Cem. Concr. Res.* **2020**, *129*, 105971. [CrossRef]
25. *C1698-09*; Standard Test Method for Autogenous Strain of Cement Paste and Mortar. ASTM International: West Conshohocken, PA, USA, 2009.
26. Methods of testing cement-Part 1: Determination of strength. In *Quality and Standards Authority of Ethiopia, ES*; European Committee for Standardization: Brussels, Belgium, 2005; p. 1176-1.
27. Melo Neto, A.A.; Cincotto, M.A.; Repette, W. Drying and autogenous shrinkage of pastes and mortars with activated slag cement. *Cem. Concr. Res.* **2008**, *38*, 565–574. [CrossRef]
28. Cao, R.; Zhang, S.; Banthia, N.; Zhang, Y.; Zhang, Z. Interpreting the early-age reaction process of alkali-activated slag by using combined embedded ultrasonic measurement, thermal analysis, XRD, FTIR and SEM. *Compos. Part B Eng.* **2020**, *186*, 107840. [CrossRef]
29. Bernal, S.A.; Provis, J.L.; Rose, V.; Mejía de Gutierrez, R. Evolution of binder structure in sodium silicate-activated slag-metakaolin blends. *Cem. Concr. Compos.* **2011**, *33*, 46–54. [CrossRef]
30. Yang, J.B.; Snoeck, D.; de Belie, N.; Sun, Z.P. Effect of superabsorbent polymers and expansive additives on the shrinkage of alkali-activated slag. *Cem. Concr. Compos.* **2021**, *123*, 104218. [CrossRef]
31. Ye, H.; Radlińska, A. Shrinkage mitigation strategies in alkali-activated slag. *Cem. Concr. Res.* **2017**, *101*, 131–143. [CrossRef]
32. Sun, Z.; Vollpracht, A. Isothermal calorimetry and in-situ XRD study of the NaOH activated fly ash, metakaolin and slag. *Cem. Concr. Res.* **2018**, *103*, 110–122. [CrossRef]
33. Runci, A.; Provis, J.; Serdar, M. Microstructure as a key parameter for understanding chloride ingress in alkali-activated mortars. *Cem. Concr. Compos.* **2022**, *134*, 104818. [CrossRef]
34. Wang, Z.; Cheng, Y.; Wang, G.; Ni, G.; Wang, L. Comparative analysis of pore structure parameters of coal by using low pressure argon and nitrogen adsorption. *Fuel* **2022**, *309*, 122120. [CrossRef]
35. Pastorino, D.; Canal, C.; Ginebra, M.P. Multiple characterization study on porosity and pore structure of calcium phosphate cements. *Acta Biomater.* **2015**, *28*, 205–214. [CrossRef]
36. Li, N.; Farzadnia, N.; Shi, C.J. Microstructural changes in alkali-activated slag mortars induced by accelerated carbonation. *Cem. Concr. Res.* **2017**, *100*, 214–226. [CrossRef]
37. Borges, P.H.R.; Banthia, N.; Alcamand, H.A.; Vasconcelos, W.L.; Nunes, E.H.M. Performance of blended metakaolin/blastfurnace slag alkali-activated mortars. *Cem. Concr. Compos.* **2016**, *71*, 42–52. [CrossRef]
38. Fu, C.; Ye, H.; Zhu, K.; Fang, D.; Zhou, J. Alkali cation effects on chloride binding of alkali-activated fly ash and metakaolin geopolymers. *Cem. Concr. Compos.* **2020**, *114*, 103721. [CrossRef]
39. Ayeni, O.; Onwualu, A.P.; Boakye, E. Characterization and mechanical performance of metakaolin-based geopolymer for sustainable building applications. *Constr. Build. Mater.* **2021**, *272*, 121938. [CrossRef]

Disclaimer/Publisher's Note: The statements, opinions and data contained in all publications are solely those of the individual author(s) and contributor(s) and not of MDPI and/or the editor(s). MDPI and/or the editor(s) disclaim responsibility for any injury to people or property resulting from any ideas, methods, instructions or products referred to in the content.